Journal of Theoretical Biology 595 (2024) 111933

Contents lists available at ScienceDirect

Journal of Theoretical Biology

journal homepage: www.elsevier.com/locate/yjtbi

The nasal cavity of the bearded seal: An effective and robust organ for retaining body heat and water

Hyejeong Lee Cheon [a], Nataliya Kizilova [b,c], Eirik G. Flekkøy [g,d], Matthew J. Mason [e], Lars P. Folkow [f], Signe Kjelstrup [g,*]

[a] Department of Physics, Norwegian University of Science and Technology, NTNU, Høgskoleringen 5, Trondheim, NO-7491, Norway
[b] PoreLab, Department of Physics, Norwegian University of Science and Technology, NTNU, Høgskoleringen 5, Trondheim, NO-7491, Norway
[c] Institute of Aeronautics and Applied Mechanics, Warsaw University of Technology, Nowowiejska 24, Warsaw, 00-665, Poland
[d] PoreLab, Department of Physics, University of Oslo, Sem Sælandsvei 24, Oslo, N-0371, Norway
[e] Department of Physiology, Development & Neuroscience, University of Cambridge, Cambridge, CB2 3EG, UK
[f] Department of Arctic and Marine Biology, UiT – the Arctic University of Norway, Framstredet 39, Tromsø, 9019, Norway
[g] PoreLab, Department of Chemistry, Norwegian University of Science and Technology, NTNU, Høgskoleringen 5, Trondheim, NO-7491, Norway

ARTICLE INFO

Dataset link: https://github.com/ hyejeonc/nose-calculations

Keywords:
Computational fluid dynamics (CFD)
Heat- and water losses
Bearded seal (*Erignathus barbatus*)
Maxilloturbinate function
Entropy production
Energy dissipation

ABSTRACT

We report the effects of varying physiological and other properties on the heat and water exchange in the maxilloturbinate structure (MT) of the bearded seal (*Erignathus barbatus* or Eb) in realistic environments, using a computational fluid dynamics (CFD) model. We find that the water retention in percent is very high (about 90 %) and relatively unaffected by either cold (−30 °C) or warm (10 °C) conditions. The retention of heat is also high, around 80 % . Based on a consideration of entropy production by the maxilloturbinate system, we show that anatomical and physiological properties of the seal provide good conditions for heat and water exchange at the mucus lining in the seal's nasal cavity. At normal values of tidal volume and maxilloturbinate (MT) length, the air temperature in the MT reaches the body temperature before the air has left the MT channels. This confers a safety factor which is expected to be helpful in exercise, when ventilation increases.

1. Introduction

The bearded seal (*Erignathus barbatus*, Eb) is a pinniped living in the Arctic and subarctic regions. Experiments on Eb have been carried out from various perspectives. Diving, haul-out, immigration, vocalization and breeding behavior have all been studied in connection with sea ice extent *e.g.* (MacIntyre et al., 2013; Escobar-Amado et al., 2022; Llobet et al., 2021; Olnes et al., 2020; Cameron et al., 2018). Food intake, metabolism and composition of body fat have been investigated with regard to moulting and lactation (Lydersen et al., 1996; Thometz et al., 2021; Foster et al., 2018).

The anatomy and physiology of Eb have also been explored *e.g.* (Mason et al., 2020; Marshall et al., 2006; Reynolds and Seaman, 1976). The tree-like, branched structure of maxilloturbinate (MT) bones that fills the nasal cavity is a striking feature of the seal nose (Negus, 1958; Moore, 1981; Hillenius, 1992). Eb has a MT structure that is more complex than that of lower-latitude species, as characterized by computed tomography (Mason et al., 2020). It was suggested that the nasal structure of Eb may have evolutionary advantages in a cold climate compared to the equivalent in seals from the subtropical region. Further support for this idea was obtained by Cheon et al. (2023). Arctic animals that live in very cold marine environments are in need of energy-efficient heat and water exchange. It is known from experiments that the complex nasal structure not only plays an important role in humidifying dry, and warming cold, ambient air before it enters the lungs, but also serves to retain heat and water on exhalation. This is the case not only in seals, (Huntley et al., 1984; Folkow and Blix, 1987), but also in reindeer (Blix and Johnsen, 1983; Langman, 1985), birds (Johansen and Bech, 1983; Blix, 2016; Westvik, 2022) and humans (Marks et al., 2019). Even the comparatively simple human nose is capable of warming and humidifying air at quite low temperatures. But the complex MT structures of the seal nasal cavity appear to be linked to a better ability to save heat and water (Negus, 1958; Cheon et al., 2023). This work aims to gain more insight on this issue. How can we characterize the ability to retain heat and water in the MT? Does the respiratory system of the seal operate with low energy loss, water loss or perhaps both? We have seen that Eb has some abilities that are superior to other seals when it comes to nasal heat and water exchange in the Arctic climate. These abilities were found to be related

* Corresponding author.
E-mail address: signe.kjelstrup@ntnu.no (S. Kjelstrup).

https://doi.org/10.1016/j.jtbi.2024.111933
Received 21 March 2024; Received in revised form 19 August 2024; Accepted 29 August 2024
Available online 10 September 2024

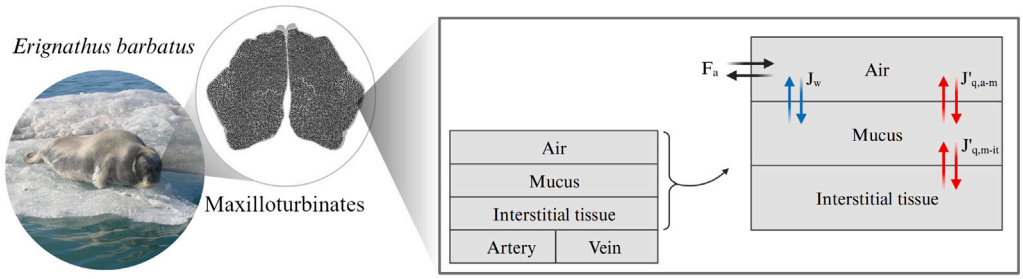

Fig. 1. Subsystems of the model. Air enters with ambient temperature and a specified relative humidity. The maxilloturbinate cross-section is shown in the inset to the left. The right-hand side of the figure illustrates the air channels, the liquid mucus layer and the interstitial tissue. Red and blue arrows indicate the heat and water fluxes, respectively, while black arrows indicate the flow of air. Fluxes are perpendicular to the air flow through the nose.

to the perimeter of the cross-sectional area for air flow (Cheon et al., 2023).

In this paper, we compute the entropy production associated with both heat and water transfer within the maxilloturbinates, over the course of a breathing cycle. In principle, if the exchange at any local position along the MT occurs without losses in water and heat, the exhaled gas would be of exactly the same temperature and relative humidity as the ambient air that was breathed in. In this situation, the overall entropy production relating to heat and mass transfer would be zero. In reality, the exhaled gas is likely to be warmer and wetter than the ambient air, and we calculate a positive value for this entropy production. It can be shown for the case of heat transport only, that a minimum in the entropy production associated with breathing means maximum overall efficiency of the heat-exchange system (Kjelstrup et al., 2017). Therefore, in this paper we consider how changing various parameters, including tidal volume and maxilloturbinate length, would affect the MT entropy production, with a view to assessing the extent to which the system is optimal. The entropy production was used to characterize the resting state of respiration. The aim was to see how this property was changing by varying physiological and environmental conditions.

Computer simulations can be used to overcome the difficulties of experiments in animals. The heat and water exchange in the nasal cavity of Arctic animals, including reindeer (Magnanelli et al., 2017; Solberg et al., 2020) and seals (Flekkøy et al., 2023; Cheon et al., 2023) have, for instance, been modeled and compared with that in mammals such as dogs (Craven et al., 2007, 2010), human (Naftali et al., 2005; Elad et al., 2008; Kim et al., 2017; Garcia et al., 2007), rats and monkeys (Ito et al., 2017). Various software, visualization techniques and numerical methods are available from these works.

The numerical model used here (Cheon et al., 2023; Magnanelli et al., 2017; Solberg et al., 2020) is a quasi 1D-model designed to investigate heat and water exchange. Diverse thermodynamic and hydrodynamic properties of the respiratory turbinate system are calculated, including the local temperature of five subsystems: air, mucus lining, interstitial tissue, artery and vein, as well as fluid flow in the mentioned five subsystems. The model utilizes water vapor–liquid interface resistivities. The phase transition of water is described as mass transport across the liquid–vapor interface, in the same manner as, *e.g.* in membrane distillation and desalination (Kjelstrup and de Koeijer, 2003; Rauter et al., 2021a,b; Wilhelmsen et al., 2016). The model of Cheon et al. has an advantage of flexibility over similar models of nasal heat exchange because it does not use commercial CFD (computational fluid dynamics) software, which is accompanied with large computational costs. It is made available for exploring new variables by new users.

In this study, we aim to investigate variables which affect the function of the MT in bearded seals (Eb), using this model. The variables considered include (i) how much air is inspired and expired per breath and (ii) how many breaths take place per minute. The first is the tidal volume. The second is the ventilation frequency. These vary depending on species, sex, age and behavior of seals (diving, foraging, hauling-out, floating on surface and sleeping) (Reed et al., 1994; Castellini et al., 1994). Although the composition of the respiratory gases will change on inspiration and expiration, the respiratory exchange ratio is taken to be 1.0. So the pressure is not affected by the breathing process. We aim to examine how energy costs associated with the heat and water exchange in the MT change, with reference to a variety of mentioned states and abilities. Relative humidity (RH) of the environment will also affect the respiratory dissipation of energy and this was not included in previous works (Magnanelli et al., 2017; Solberg et al., 2020; Cheon et al., 2023). We focus on how relative humidity conditions alter entropy production and energy dissipation. We shall see how the functioning of the MT depends on its structure and boundary conditions.

The paper is structured as follows. We first give the anatomical and functional properties needed to model the MT of the bearded seal (Section 2). In the *Methods* section (Section 3), we present the theoretical model. The numerical results are interpreted and analyzed in Section 4, *Results and Discussion*. Additional information related to calculations is included in *Appendix*.

2. System

2.1. Maxilloturbinate structure and function

The seal has a dendritic MT morphology. The ambient air, of given temperature and humidity, passes the nasal passage where it is humidified and warmed to body temperature. The saturated and warmed air is next exhaled and heat is transferred from the air to the cool mucus lining. This thin mucus layer is overlying the epithelial cell tissue on the MT bone. During this ventilation process, heat and water in the air are exchanged with the heat and water in the mucus lining of the MT in a temporal counter-current fashion as described by Jackson and Scmidt-Nielsen (1964). The process is indicated in Fig. 1 by arrows. Supplementary heat- and mass transfer processes between subsystems are also depicted. We have earlier shown (Cheon et al., 2023) that it is sufficient to consider three subsystems, the air flow channel, the mucus lining (water properties assumed) and the interstitial tissue (blood properties assumed). The simplified system will thus be used here.

2.2. Anatomy and physiology

Mason et al. (2020) observed associations between nasal structure complexity and the latitude of seal habitat. They proposed that the climatic environment induced adaptations in MT morphology. That of *Erignathus barbatus*, Eb, was reported. The Eb model has now been used in several studies (Flekkøy et al., 2023; Cheon et al., 2023), and is therefore chosen for in-depth studies here.

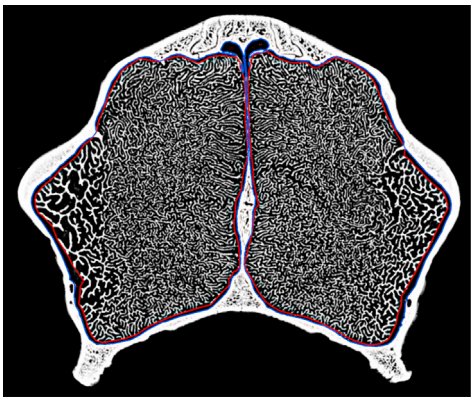

(a) CT scan image (tomogram) in the transverse plane through the middle of the maxilloturbinate mass, encircled by a red line. The blue line shows the boundary of the nasal cavity.

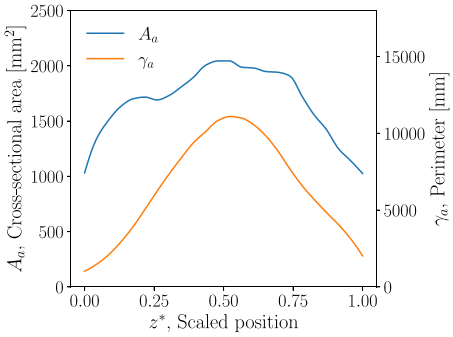

(b) Cross-sectional area and perimeter (A_a and γ_a) as a function of the scaled position computed from CT-data.

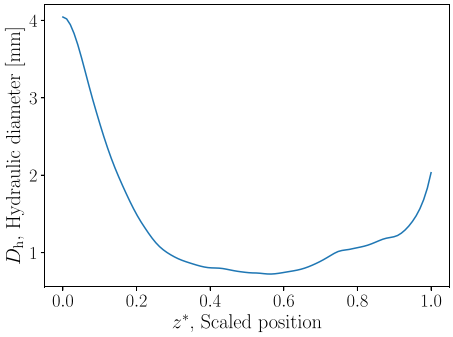

(c) Hydraulic diameter as a function of the scaled position calculated from variables in (b).

Fig. 2. Reconstructed CT scan image of the MT of *Erignathus barbatus* (a) and anatomical data (b and c) replotted from Cheon et al. (2023).

Fig. 2 shows the morphology of the MT structure from various perspectives. Fig. 2a shows a computed tomogram cross-section through the skull, in the densest MT region. The MT geometry can be characterized by the cross-sectional area of the airways (the air contained within the mass) and the MT perimeter, denoted A_a and γ_a, respectively. It does not include the air surrounding the MT mass or between left and right masses. Their variations among the MT, shown in Fig. 2b, were calculated from CT-scans of prepared skulls, in which the interstitial tissue lining of the MT bones was either substantially shrunk or missing. This means that the values are essentially based on the bony MT structure.

The cross-sectional area for airflow and the perimeter are used to compute the hydraulic diameter $D_h = A_a/\gamma_a$ (Mason et al., 2020) in Fig. 2c. The D_h is a measure of the narrowness of the passageways.

The air pathway in the MT has the length L in the direction of airflow. We see from 2b that the MT structure is particularly elaborate in the center of the MT, where $0.2 < z^* < 0.8$ and $z^* = z/L$ is the dimensionless coordinate axis along the nasal duct.

Other variables of the present model are estimates for Eb based on physiological data from other phocid seal species in the literature, for a hypothetical 180 kg animal. All these variables are listed in Table 1, but further explained elsewhere (Cheon et al., 2023).

The MT porosity of Eb, ϕ, was estimated from the volume of the MT excluding bony parts, V_{void}, over the total volume, V_{tot}. The volume was calculated using the length and the average cross-sectional area of MT excluding bony parts, 20.3 cm^2 (Flekkøy et al., 2023). This gives $\phi = 0.55$, an average value which we can use for the whole of the MT mass.

3. Methods

Before the solution procedure was started, transport coefficients were calculated according to physiological, physical and chemical conditions. Coefficients were compatible with the form dictated by the theory of non-equilibrium thermodynamics, *i.e.*, Eqs. (11) and (12). The driving forces were expressed, after composition and temperature profiles were obtained, allowing the determination of the entropy production according to Eq. (13).

The quasi 1-dimensional CFD model, used to simulate the MT function, was originally formulated by Magnanelli et al. for applications to reindeer (Magnanelli et al., 2017). It was adapted the model to seals by Cheon et al. (2023). Cheon et al. showed that the temperature profiles of the arteries and veins were similar to those of the interstitial tissue, giving us reasons to simplify the model and omit the veins and arteries result here. The revised system consists now of three subsystems as shown on the right-hand side in Fig. 1. The equations to be solved are those of the three subsystems; air, mucus lining and interstitial tissue.

The model used in this investigation was first developed for reindeer (Cheon et al., 2023). It was recently adapted to seals by Cheon et al. (2023), and the Supplementary Material of that paper fives details of the solution procedure. Here we only note that the problem is time dependent (videos of the breathing cycles were presented earlier). The balance equations for each subsystem and their numerical solution can be found in the works of Cheon et al. (2023), Magnanelli et al. (2017). We repeat the central equations for convenience. They show how the cross-sectional area of the airway passage, A_a, and its perimeter, γ_a, enters the calculations.

Table 1
Anatomical and physiological data for a hypothetical 180 kg bearded seal (Eb). Physiological data that were not available for Eb were measured in gray seals (*Haliochoerus grypus*) (Reed et al., 1994; Folkow and Blix, 1987; Folkow et al., 1988) or northern elephant seals (*Mirounga angustirostris*) (Huntley et al., 1984) of equal size. The A_a and γ_a vary with scaled position, z^*, so we present maximum values, $A_{a,max}$ and $\gamma_{a,max}$.

Variable	Description	Value	Literature
V_t	Tidal volume	6.3 dm^3	Reed et al. (1994)
f_a	Breathing frequency	19.4 min^{-1}	Reed et al. (1994)
t_{br}	Duration of one ventilatory cycle	3.09 s	Reed et al. (1994)
L	Maxilloturbinate length along the z-axis	6.10×10^{-2} m	Mason et al. (2020)
$A_{a,max}$ [a]	Max. cross-sectional area	3.55×10^{-3} m^2	Cheon et al. (2023), Flekkøy et al. (2023)
$\gamma_{a,max}$	Max. perimeter	11.1 m	Cheon et al. (2023), Flekkøy et al. (2023)
T_{body}	Body temperature	36 °C	Folkow and Blix (1987)
T_{amb}	Ambient temperature	−30/10 °C	Folkow and Blix (1987), Huntley et al. (1984)
RH_{body}	Relative humidity of deep body	1.00	Folkow and Blix (1987), Huntley et al. (1984)
RH_{amb}	Relative humidity of ambient air	0.20/0.50/0.90	Folkow and Blix (1987), Naftali et al. (2005)
$c_{p,b}$	Specific heat capacity of blood	4500 J kg^{-1} K^{-1}	Magnanelli et al. (2017)
ρ_b	Density of blood	1000 kg m^{-3}	Magnanelli et al. (2017)
k_b	Thermal conductivity of blood	0.50 J m^{-1} s^{-1} K^{-1}	Magnanelli et al. (2017)
$c_{p,m}$	Specific heat capacity of mucus	4200 J kg^{-1} K^{-1}	Magnanelli et al. (2017)
ρ_m	Density of mucus	1000 kg m^{-3}	Magnanelli et al. (2017)
k_m	Thermal conductivity of mucus	0.60 J m^{-1} s^{-1} K^{-1}	Magnanelli et al. (2017)
d_m	Mucus thickness	1.0×10^{-5} m	Bush et al. (1998), Kaulbach et al. (1993)
d_{it}	Interstitial tissue thickness	2.0×10^{-4} m	Folkow et al. (1988)
F_b	Mass flow of blood	2.2×10^{-4} kg min^{-1}	Magnanelli et al. (2017)

[a] The value was taken from Fig. 2 in Cheon et al. (2023), correcting their incorrect Table 1 value (2.03×10^{-3} m^2 as shown in Fig. 2C).

3.1. Energy and mass-balances

The energy balance for a volume element in the air subsystem, the energy balance is written as

$$A_a\rho_a c_{p,a}\frac{\partial T_a}{\partial t} = -F_a c_{p,a}\frac{\partial T_a}{\partial z} - \gamma_a J'_{q,a\text{-}m} - \gamma_a J_w(h_{w,a} - h_a) + A_a\rho_a\sum_i h_i\frac{\partial w_i}{\partial t} - F_a\sum_i h_i\frac{\partial w_i}{\partial z}, \quad (1)$$

where A_a and γ_a were defined above, ρ_a is the density of the air, T_a is the temperature of the air, t is the time and $c_{p,a}$ is the specific heat capacity of air. The flow F_a is the total mass flow in the z-direction across the MT, where h_i is the specific enthalpy of the ith component, $h_{w,a}$ is the specific enthalpy of water vapor and h_a is the specific enthalpy of air. The mass fraction of component i, w_i, is the ratio of the ith component mass and the total mass of the air, including the ith component. The expression $\partial w_i/\partial z$ is the change in mass fraction in the z-direction. The left-hand side of the equation describes the temperature change in the volume element, while the right-hand side describes fluxes in and out of the element of conducted and latent heat. The measurable heat flux, $J'_{q,a\text{-}m}$, is positive when directed from the air to the mucus lining subsystem.

The water mass flux from the air to the mucus lining is J_w, positive for condensation and negative for evaporation.

The energy balance of the mucus lining (superscript m) is described similarly. We obtain:

$$A_m\rho_m c_{p,m}\frac{\partial T_m}{\partial t} = \gamma_m(J'_{q,a\text{-}m} + J_w(h_{w,a} - h_{w,m})) - \gamma_m J'_{q,m\text{-}it}, \quad (2)$$

where T_m is the temperature of the mucus lining and A_m is the cross-sectional area which the mucus occupies, ρ_m is the density of mucus and $c_{p,m}$ is the specific heat capacity of the mucus. We have assumed that all physical properties of the mucus are the same as those of water. Other mucus variables (subscript m) are defined in the same way as the corresponding variables in the air subsystem. The $h_{w,m}$ is the specific enthalpy of liquid water in the mucus lining and $J'_{q,m\text{-}it}$ is the measurable heat flux from mucus lining to the interstitial tissue.

From mass conservation, the mucus water mass flux is constant across the lining; $J_w = -J_m$ where J_m is the mass flux of water into the underlying epithelial tissue.

The energy balance of the interstitial tissue (subscript it) is finally,

$$A_{it}\rho_{it}c_{p,b}\frac{\partial T_{it}}{\partial t} = \gamma_m J'_{q,m\text{-}it} - \gamma_{art}J'_{q,it\text{-}art} - \gamma_{ven}J'_{q,it\text{-}ven}, \quad (3)$$

where T_{it} is the temperature of the interstitial tissue, ρ_{it} is the density of the blood, $c_{p,b}$ is the specific heat capacity of blood. $J'_{q,it\text{-}art}$ is the measurable heat flux from the interstitial tissue to the artery in the r-direction, $J'_{q,it\text{-}ven}$ is the measurable heat flux from the interstitial tissue to the vein in the r-direction. Here we assume that all physical properties of the interstitial tissue are the same as those of blood.

All variables defined above are averaged over the cross-sectional area, given for a point on the z-axis along the length of the nose cavity. This way of modeling follows the standard procedure for chemical reactors (Johannessen and Kjelstrup, 2004; Magnanelli et al., 2017; Solberg et al., 2020; Cheon et al., 2023). For more details, see Cheon et al. (2023), supporting materials and the GitHub link provided.

The net amount of heat and water retained in the turbinate system was estimated from these results following (Blix and Johnsen, 1983). The net amount of water vapor, $M_{w,add}$, was calculated by subtracting the amount of water vapor entering the nose in the ambient air during inhalation from the amount of water vapor entering the nose from the lungs during exhalation:

$$M_{w,add} = \int_{ex}(-F_{w,a})_{z=L}dt - \int_{in}(F_{w,a})_{z=0}dt, \quad (4)$$

where $F_{w,a}$ is the mass flow of water vapor in nasal air. The absolute amount of water recovered, $M_{w,rec}$, was obtained by subtracting the amount of air flowing out through the nostrils during exhalation from the amount of water vapor entering the nose from the lungs during exhalation as,

$$M_{w,rec} = \int_{ex}(-F_{w,a})_{z=L}dt - \int_{ex}(-F_{w,a})_{z=0}dt. \quad (5)$$

The fractional recovery of water is $M_{w,rec}/M_{w,add}$. The heat recovery is captured in a similar way as for water. The heat added to the turbinate system (Q_{add}) is the sum of the heat that is necessary to warm up the inhaled air to the body temperature and the heat that is necessary to evaporate the water added during inhalation:

$$Q_{add} = \int_{in}F_a c_{p,a}(T_{body} - T_{amb})dt + M_{w,add}h_{w,lat}, \quad (6)$$

Here F_a is the air mass flow, $c_{p,a}$ is specific heat capacity of air and $h_{w,lat}$ is the latent heat of evaporation of water. The amount of recovered heat

during exhalation (Q_{rec}) is obtained as the sum of sensible heat that is subtracted from the air during exhalation, and the latent heat that is released by condensing of water, giving

$$Q_{\mathrm{rec}} = \int_{\mathrm{ex}} F_{\mathrm{a}} c_{\mathrm{p,a}} (T_{\mathrm{body}} - T_{\mathrm{ex}}) dt + M_{\mathrm{w,rec}} h_{\mathrm{w,lat}}, \tag{7}$$

where T_{ex} is the exhaled air temperature and the fractional recovery of heat is $Q_{\mathrm{rec}}/Q_{\mathrm{add}}$. These flows at the nose boundaries do not contribute to the entropy production inside. They can be used to estimate heat and water retention in the organ as a whole, with the assumption that other losses of heat and water at the system boundaries are small.

3.2. The entropy balance

The entropy production in a system is a measure of the generalized friction in a process. It can therefore be used to measure the efficiency of a particular process (Kjelstrup et al., 2017). The entropy production is zero when the process is fully reversible.

Because the entropy production, σ, is characteristic of the way the process takes place, it quantifies and measures where energy losses take place. It can be used to compare organ performance under various conditions. Fluxes, J, giving rise to entropy production, were shown as arrows in Fig. 1. The product sum fluxes and corresponding driving forces, X, is equal to the entropy production. By multiplication with the temperature of the surroundings, we obtain the energy dissipation, W_{lost} (Kjelstrup et al., 2017) of the adsorption/desorption processes at the convoluted surfaces in the nose cavity. We have:

$$\sigma = \sum_i \gamma_i J_i X_i \geq 0 \qquad \text{for} \quad i \in \{q, w\}, \tag{8}$$

Here q, w stands for local heat and water transport, respectively. Details for the construction of σ can be found in the cited literature. Here we are sketching the set of relevant forces for the discrete description:

$$X_q = \Delta\left(\frac{1}{T}\right), \tag{9}$$

$$X_w = -\frac{1}{T}\Delta\mu + h_{\mathrm{w,a}}\Delta\left(\frac{1}{T}\right) \tag{10}$$

where μ is the chemical potential and $h_{\mathrm{w,a}}$ is the specific enthalpy of water vapor. A linear relationship follows for forces and fluxes,

$$R_{qq} J'_q + R_{qw} J_w = X_q \tag{11}$$

$$R_{wq} J'_q + R_{ww} J_w = X_w \tag{12}$$

where R_{qq}, R_{ww}, R_{qw} and R_{wq} are resistivity coefficients. The coupling coefficients are the same, $R_{qw} = R_{wq}$ (Onsager's reciprocal relations). The measurable heat flux is J'_q and J_w is the water flux.

The total entropy production of the breathing process in the nose cavity, Σ, is the integral of σ over the length coordinate.

$$\Sigma = \int_{\mathrm{in}} \sigma dt + \int_{\mathrm{ex}} \sigma dt \geq 0, \tag{13}$$

where in and ex stand for the durations of inhalation and exhalation respectively. The entropy production is always positive. In the present case, the total entropy production is obtained by integrating over the adsorption/desorption processes perpendicular to the z-axis. Contributions from viscous dissipation in shear flow in the nose are neglected. The entropy production in a system is computed directly from Eq. (13) with an explicit expression for σ. The dissipated energy is according to the Guy–Stodola theorem the production of the integral, Σ, and the temperature of the ambient.

At steady state, the energy dissipation in the nose, $T_{\mathrm{amb}}\Sigma$, is also delivered to the environment. The heat lost by advection through the nose must come from the metabolism in the whole animal.

In a system in steady state and with perfectly isolated walls, the entropy production inside (Σ) is equal to the net entropy flow out of the system. In the present case, the system (the MT) is quasi-stationary and not isolated, as heat is transported into the surroundings perpendicular to the air flow direction (into the veins and arteries).

An earlier model (Flekkøy et al., 2023) did not separate between contributions of water and heat transport. To some extent this has been done now, because the present model does not assume thermodynamic equilibrium at the MT wall.

3.3. The breathing cycle

Although breathing in seals is typically intermittent (*e.g.* Reed et al., 1994), our model for simplicity assumes that the mass flow rate of the air, F_{a}, is a sinusoidal function of time, t, during eupnea. We further assume that the overall interval between inspiration events, 3 s, is the period of the sinusoid, ignoring the pauses in breathing that were actually observed in the Reed et al. study. This can be written as,

$$F_{\mathrm{a}} = F_{\mathrm{a,max}} \sin 2\pi \left(\frac{t}{t_{\mathrm{br}}}\right), \tag{14}$$

where $F_{\mathrm{a,max}} = \rho_{\mathrm{a}} V_{\mathrm{T}}/t_{\mathrm{br}}$ is the maximum airflow in a breathing cycle of duration t_{br}. This flow is proportional to the tidal volume, V_{T}. The breathing frequency is a more important variable for regulating ventilation than the V_{T} in diving animals, since they maintain relatively high V_{T} compared to non-diving mammals. The V_{T} is, as a default, less variable than in, for example, humans. The range covered in this investigation will therefore include all possible variations.

3.4. Boundary conditions

We shall study the effects on heat and water exchange of the modeled changes of tidal volume, V_{T}, breathing frequency, f_{a}, and length, L, of the MT along the z-axis. The properties affect the balance equations, Eq. (1) and Eq. (2), via Eq. (14). The set of equations was solved as described by Magnanelli et al. (2017), Solberg et al. (2020), Cheon et al. (2023) for new boundary conditions, ambient temperature, T_{amb}, and relative humidity, RH, as listed in Table 1. The boundary conditions are:

During inhalation,	During exhalation,
• RH($z^* = 0$): 0.20, 0.50, 0.90	• RH($z^* = 1$): 1.00
• $T_{\mathrm{a}}(z^* = 0) = T_{\mathrm{amb}}$.	• $T_{\mathrm{a}}(z^* = 1) = T_{\mathrm{body}}$.
• $T_{\mathrm{m}}(z^* = 1) = T_{\mathrm{body}}$.	• $T_{\mathrm{m}}(z^* = 1) = T_{\mathrm{body}}$.
• $T_{\mathrm{it}}(z^* = 1) = T_{\mathrm{body}}$.	• $T_{\mathrm{it}}(z^* = 1) = T_{\mathrm{body}}$.
• $T_{\mathrm{art}}(z^* = 1) = T_{\mathrm{body}}$.	• $T_{\mathrm{art}}(z^* = 1) = T_{\mathrm{body}}$.
• $T_{\mathrm{ven}}(z^* = 0) = T_{\mathrm{art}}(z^* = 0)$.	• $T_{\mathrm{ven}}(z^* = 0) = T_{\mathrm{art}}(z^* = 0)$.

Here z^* is the scaled position where $z^* = 1$ stands for the position of a MT at the proximal end and $z^* = 0$ implies the distal end such as nostrils. The temperatures T_{ven} of the vein subsystem and T_{art} of the arteries were computed, but are not shown.

The energy balances of each subsystem provide a set of five partial differential equations, see Magnanelli et al. (2017), for a more detailed description. Together with the mass and entropy balance, there are seven partial differential equations to solve. We transform the system of partial differential equations into a set of ordinary differential equations by discretizing in the spatial dimension. Here 24 discretization points were chosen for the z-dimension, and in each of these grid points we approximated the first-order spatial derivatives using a finite difference method (MatLab routines "dss020"), see Cheon et al. (2023). Thus, every partial differential equation was transformed into a set of 24 ordinary differential equations in time. In order to account for boundary conditions, we replaced the corresponding differential equations with the algebraic equations as given by the boundary conditions below. Thus, we obtained a final set of ordinary differential and algebraic equations that were solved using the solver "ode15s", in combination with a mass matrix.

Table 2
Overview of results, Cases 0–7. The total entropy production Σ of the MT in Eb is given in each case. Values are shown for half and double the values of the reference value of V_T, f_a and L. RH means relative humidity.

Case	Environmental conditions; Variables	Entropy production of MT/JK^{-1}cyc^{-1}
0	Cold-wet; T_{amb}= −30 °C, RH = 0.90	0.047
1	Cold-dry; T_{amb}= −30 °C, RH = 0.20	0.101
2	Warm-wet; T_{amb}= 10 °C, RH = 0.90	0.004
3	Warm-dry; T_{amb}= 10 °C, RH = 0.20	0.022
4	Cold-medium, T_{amb}= −30 °C; RH = 0.50	0.074
5	V_T variation; 0.5V_T/Case 0/2V_T	0.048/0.047/0.055
6	f_a variation; 0.5f_a/Case 0/2f_a	0.092/0.047/0.024
7	L variation; 0.5L/Case 0/2L	0.059/0.047/0.040

The inherently dynamic problem, elapses after a sufficient time in a pseudo-steady state, where the thermodynamic variables have the same values at corresponding times of consecutive breathing cycles. A video of the breathing cycle can be found in Cheon et al. (2023). In a stable state, the results should not depend on the set of initial conditions. In practice, we stopped the calculations when the difference between temperatures at corresponding times of two consecutive breathing cycles was smaller than 0.01 K. This condition was reached after about eleven days, making the choice of discretization a practical one.

3.5. Case studies

The results of all variations will be compared to a reference, Case 0, which is the bearded seal (Eb) living under Arctic *cold and humid* conditions. The temperature is T_{amb}= −30 °C and the relative humidity is RH = 0.90. This condition was also used in our comparative studies, see Cheon et al. (2023). The new cases include two types of variations; (i) variations in the environment (Cases 1–4) and (ii) variations in physiological parameters (Cases 5–7), see Table 2. The cases are designed to offer more insight into the energy efficiency of the heat and water exchange processes in the MT of Eb.

4. Results and discussion

The results for heat and water losses as well as for the entropy production of water- and heat exchange in the MT of Eb are presented in Tables 2, 3, 4 and 5, and in Figs. 3–6. We distinguish between five cases called cold-wet, cold-medium, cold-dry, warm-wet and warm-dry where we have considered 10 °C to be 'warm' for an Arctic animal. The cases are characterized by the environmental conditions applied, even if the seal is a marine animal living under wet conditions. An overview of the results for the entropy production is given already in Table 2, but numbers are discussed in Section 4.3. We discuss first the approximations made in the model (Section 4.1), before we present and discuss results for the breathing cycle (Sections 4.2–3); implications for the energy budget (Section 4.4) and the performance away from the common conditions (Sections 4.5-6).

4.1. Model properties

The properties of the breathing cycle were computed under some assumptions which need be considered in the interpretation of results. We first note that the temperature variations in the arteries and veins were, in good approximation, the same as in the interstitial tissue, which means numbers are the same within the accuracy of the calculation within 1 % (Cheon et al., 2023). Neglecting the difference leads to a small, systematic underestimation of the entropy production at the mucus lining.

It is known that the nose tip/nostrils in reality are supplied with blood vessels that are anatomically separate from those supplying the MT (Folkow et al., 1988). The effect was modeled by Flekkøy et al. (2023). Such a heat source may also add a systematic contribution to the entropy production. We did not include any extra heat source in the model for reasons of simplicity. It can in principle be included, for example by introducing an extra heat source on the right-hand side of Eq. (2). Introduction of a heat source will produce temperature profiles at the inlet which are closer to experimental results.

Earlier studies have been divided over the issue of turbulence of laminar airflow in the turbinate. Flekkøy et al. (2023) considered laminar airflow. Others Folkow and Blix (1987), Solberg et al. (2020), Cheon et al. (2023) assumed turbulent flow. Turbulent flow conditions in the nose will possibly lower the thermal conductivity and raise the outlet temperature. The choice has an impact on the heat transfer coefficient and therefore the temperature profiles inside. Better heat transfer (turbulent conditions) means a lower entropy production in the mucus lining. Such conditions were used by Magnanelli et al. (2017) in the modeling of the reindeer nose. As the local conditions are unknown at present, we choose here for laminar conditions which gives better separation of profiles. We found that turbulent flow conditions did not produce temperature profiles that differed much from those reported before. They were found to give a temperature difference not larger than 2 °C above that of laminar flow when measured at the distal end.

In view of the uncertainties introduced by these simplifications, we are reporting numbers to two significant figures. Emphasis is put on trends in results rather than on absolute values.

Table 3
Heat loss and heat recovery for T_{amb} = −30 (cold), T_{amb}= 10 °C (warm), and RH = 0.90 (wet), RH = 0.20 (dry) conditions for Cases 0-3.

	Seal condition			
	Cold-wet	Cold-dry	Warm-wet	Warm-dry
Heat loss/J cyc^{-1}	954	1075	571	402
Heat loss/W	316	355	190	134
Heat recovery/%	72	68	70	81
Heat loss/water loss kJ mg^{-1}	22	17	5	6

Table 4
Water loss and water recovery for T_{amb} = −30 °C (cold), T_{amb}= 10 °C (warm) and RH = 0.90 (wet), RH = 0.20 (dry) conditions for Case 0-3.

	Seal condition			
	Cold-wet	Cold-dry	Warm-wet	Warm-dry
Water loss/mg cyc^{-1}	0.044	0.062	0.120	0.064
Water recovery/%	95	93	79	91

4.2. Heat and water exchange along the MT

Consider the heat- and water exchange in the MT, the primary function of the MT. The amounts of water and heat recovered in a breathing cycle were computed as described in the Method section. Changes are given per breathing cycle as well as per second in Tables 3–4. The duration of one cycle was initially set to 3 s. The cycle duration is further discussed in Section 4.4.

The heat as well as water retention are both amazingly high, as shown by Tables 3 and 4, when measured in percentage of the total amounts. The percentage recovery varies between 68 and 81% for

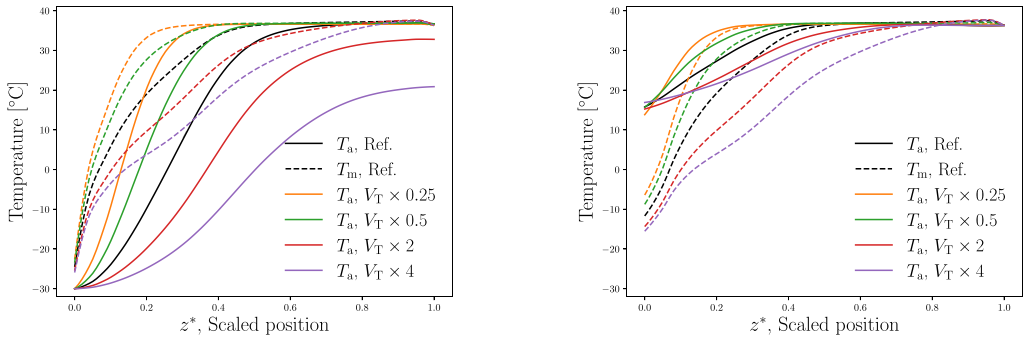

(a) $t^* = 0.25$. (b) $t^* = 0.75$.

Fig. 3. Temperature profiles of air (solid line) and mucus (dashed line) subsystems due to V_T variation when the airflow is at maximum for (a) inhalation, $t^* = 0.25$ and (b) exhalation, $t^* = 0.75$.

Table 5
Total entropy production (Σ) and dissipated energy (W_{lost}) in the MT system when $T_{amb} = -30$ °C (cold), $T_{amb} = 10$ °C (warm) and RH = 0.90 (wet), RH = 0.20 (dry) conditions for Cases 0-3.

	Seal condition			
	Cold-wet	Cold-dry	Warm-wet	Warm-dry
Entropy production (Σ)/JK^{-1}cyc^{-1}	0.047	0.101	0.004	0.022
Energy dissipation (W_{lost})/J cyc^{-1}	11	24	1.0	6.0
Energy dissipation (W_{lost})/W	4.6	8.0	0.33	2.0

heat, and 79 and 95% for water. The percentage of water retention is *always* higher, by approximately 10%. Also, the percentage water recovery is highest in cold conditions, *cf.* Table 4. This is not surprising if we consider the exponential increase of saturated vapor pressure with temperature. It may be easier to capture a small amount of water than a large. The amazingly high retention percentage for water in the MT, for warm and cold conditions alike, was also observed before (Cheon et al., 2023). Seals are in reality not much exposed to dry conditions. Such conditions were applied here to investigate its consequences.

Given that the percentage values for water retention under cold conditions are not that much different than under warm conditions, it is interesting to compute the heat loss per milligram of water loss in a cycle. These results are given in the bottom row of Table 3. A clear message appears; the number of joules lost per mg water lost is about four times higher in cold conditions than in warm (compare numbers 22 and 17 with numbers 5 and 6). The heat loss may, not surprisingly, be a critical factor at low temperatures.

4.3. The entropy production

Table 5 (see also the overview in Table 2) presents the entropy production of the mucus lining during breathing, for chosen values of ambient temperature and relative humidity (RH). This allows us to discuss the performance of the MT system at the mucus lining, *e.g* in the adsorption/desorption process. The entropy production is a measure of energy costs which are frictional costs in a generalized sense. The ideal case has zero entropy production. In this case there is equilibrium at the mucus lining everywhere. The exhaled gas has then exactly the same temperature and relative humidity as the air breathed in. Any deviations in the temperature and composition of the exhaled gas leads to (positive) entropy production, and is a measure of how far we are from ideality.

We see from Table 5 that the dissipation from heat and water transport in the cold (11 and 24 J cyc^{-1}), is much larger than the dissipation in warm conditions (1.0 and 6.0 J cyc^{-1}), on the average five times larger. The results for cold-medium conditions position themselves between cold-wet and cold-dry (cf. Table 2). We explain the difference between cold and warm conditions by different driving forces in Eqs. 9 and 10. The driving forces become larger when the environmental temperature and relative humidity sinks. The dissipation from heat and water transport at cold conditions is therefore, relatively speaking, more important for the energy budget. The results are in line with the heat losses in Table 3.

From the dependence of the entropy production on the perimeter of the cross-sectional area in the MT, we previously concluded (Cheon et al., 2023) that the MT-structure seems to be tailored for an efficient breathing process under cold conditions. This was concluded by comparing the entropy production of the monk seal MT to that of bearded seal MT, both under Arctic conditions. The entropy production in the MT of Eb under cold conditions is an indicator of the total performance of the whole system.

4.4. Resting state energy considerations

The numbers for the respiratory heat loss (from 134 to 355 W) in Table 3 are large. How can we understand them in terms of metabolic rates? A 'back-of-the-envelope' calculation may set the numbers into perspective.

Consider therefore a 180 kg seal, as used here. It has a metabolic rate in the order of 160 W in the resting state (Folkow and Blix, 1987), which increases to about 400 W when the seal becomes active. The energy cost of ventilation, i.e. the cycle costs, must be related to the fact that seals are intermittent breathers. A seal may only take some 20 breaths over a period around 5 min (made up of 3.8 min of diving and 0.8 min at the surface Reed et al., 1994). With cycle costs of say 500 J/cycle, the overall ventilation cost would be 33 W. Such a value has support from experimental data on total heat loss rates in gray seals, see Table 1 in Folkow and Blix (1987). From these data, the ventilation cost in a gray seal, scaled to 180 kg, becomes 20 W in the resting state.

The experimental values reported were found to be surprisingly independent of the air temperature (Folkow and Blix, 1987), indicating that there is an active thermoregulatory component to the nasal heat exchange mechanism. The real cycle duration is more like 2 s for the inhalation — and exhalation, with a 1 s pause before the next breath (not sinusoidal) (Reed et al., 1994). The 20 W is within an order of magnitude of the dissipation computed from the entropy production in Table 5.

An evolutionary pressure to expand the perimeter of the airflow cross-sectional area will act to improve conditions for heat and water transfer. The heat retention is percentage-wise lower than the water

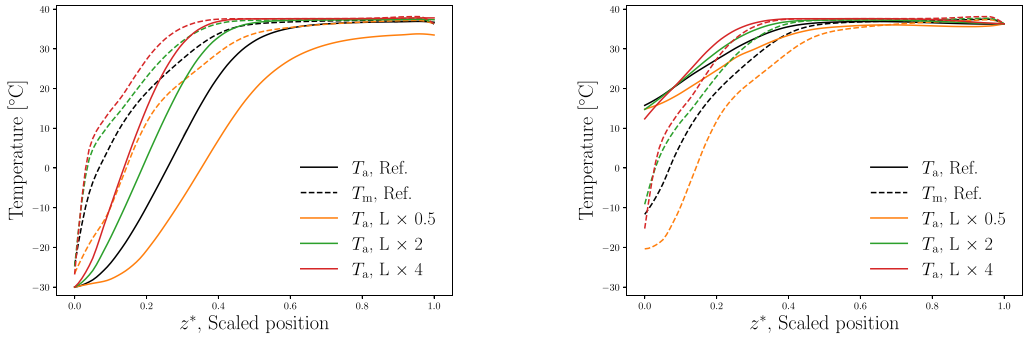

(a) $t^* = 0.25$. (b) $t^* = 0.75$.

Fig. 4. Temperature profiles of air (solid line) and mucus (dashed line) subsystems regarding L variation when (a) $t^* = 0.25$ and (b) $t^* = 0.75$; airflow is at maximum.

retention, and is also relatively costly in terms of entropy production, as explained above. We estimated earlier (Flekkøy et al., 2023) that the viscous dissipation (energy dissipated by flow in a pressure gradient) was less than 1 W. According to Kings et al. (2023) the porosity of MT is 0.8 for monk seals, 0.71 for gray seals and 0.75 for harp seals (Kings et al., 2023). Bearded seals, with porosity 0.55, have the most elaborate MT structure among the mentioned seal species. A (further) reduction in the Eb value below 0.55 may benefit both heat and water exchange at the wall. It may not be possible to continue reducing this value, however, because the further narrowing of channels would lead to increased viscous dissipation, i.e. resistance to airflow. This points to a trade-off between thermal and viscous dissipation.

4.5. Temperature gradients in the MT

The results may be used to argue that the parameters used in the default model of the MT structure in Eb, here called Case 0, reflect a robust solution to the problem of nasal heat and water retention.

We recapitulate how we may understand the breathing process of Eb under Case 0 conditions. These are the cold and humid Arctic winter conditions. Fig. 3 shows a snapshot of the temperature profiles in the airways of this seal during inhalation and exhalation. The black line represents Case 0. Fig. 3A shows inhalation profiles at time $t^* = 0.25$, while Fig. 3B shows exhalation at $t^* = 0.75$. Recall that the dimensionless time t^* measures the fraction of the breathing cycle, and that the snapshots are taken at times when the sinusoidal airflow is at its maximum. The black dashed lines show the corresponding temperature profiles in the mucus lining. We see that the mucus temperature is higher than the air temperature upon inhalation, while it is lower than the air temperature upon exhalation. Such behavior was already observed (Cheon et al., 2023) and was used to argue that the model is realistic: The incoming cold, dry air is warmed and humidified upon inhalation (Fig. 3A), but cooled and dehumidified upon exhalation (Fig. 3B).

We now observe that the rise in the mucus temperature profile in Fig. 3A takes place before we are halfway into the MT. The decline upon exhalation in Fig. 3B also takes place within this part of the MT. This confinement of the gradient to within the MT is beneficial for the seal. It is good for the inhalation function, that the core body temperature is reached with a good safety margin, *i.e.* well before the air reaches the end of the MT and merges into the nasopharynx. Such a situation has also been found in humans (Hanna and Scherer, 1986). This protects the lungs from cold air.

4.6. Breathing frequency and amplitude of flow

In the present model, the tidal volume, V_T used in this investigation to compute the amplitude of the breathing velocity, was measured at body temperature and pressure at saturated vapor conditions (Reed et al., 1994). The property has a direct impact on the airflow, F_a, in Eq. (14). We see from Fig. 3 that changes in V_T lead to significant changes in the different temperature profiles, for all cases chosen, when we compare to the reference case. Temperatures change, both in the air and in the mucus lining. A reduction in V_T by a factor two or four (cf. the orange and green solid lines), shifts the transition from cold to warm, to a position much closer to the anterior entrance of the MT. When, on the other hand, V_T is doubled or quadrupled (cf. the red and purple solid lines), we see in Fig. 3A that the air is no longer fully heated to the core body temperature measured at $z^* = 1$, the inner end of the MT. This means that an airflow that is too rapid is clearly not as effective for the exchange of heat and water between the air and mucus subsystems. However, the expired air temperature in Fig. 3B, as obtained by extrapolation of the curves to the axis (at $z^* = 0$) gives a value close to 15 °C regardless of V_T in Fig. 3B. The particular choice of boundary conditions (see the *Method* section) must be remembered to understand this. At high V_T -conditions the innermost MT temperature does not reach body temperature on inhalation. The temperature here is set to body temperature on exhalation, however (set boundary conditions). The model therefore breaks down. The situation for the animal can become dangerous since there is a constant cooling of the interior of the body.

The ability of the seal to heat the incoming air to the proper temperature may be expressed by the position of the inflection point of the air temperature profile. The inflection point is the point where the second derivative to the curve is zero. Recall that V_T affects the derivative of the temperature through the air mass flow, F_a, in Eqs. (1) and (14). We see that an increase in the value of V_T to $2V_T$ and $4V_T$ shifts the inflection point in Fig. 3A from $z^* = 0.35$ to 0.44. Already a doubling of V_T does not allow the air to reach the core body temperature. We have taken a value for V_T as measured for swimming seals breathing at the surface between dives (Reed et al., 1994). This Case 0 is robust as a reference, as the curve close to the reference value is rather flat.

4.7. Length of maxilloturbinates

The effect of a changing MT length relative to the real MT length of the Eb seal is shown in Fig. 4. The length of the reference case was multiplied by factors of 0.25, 0.5, 2 and 4, respectively. The artificial MT systems become then rather short or rather long. The corresponding temperature profiles for inhalation and exhalation are plotted in Fig. 4. When the length of a MT system is too short, as is the case with $L \times 0.25$, we found an unstable temperature profile, the reason being that the inhaled air fails to reach the core body temperature (results not shown). When the absolute length of L is longer than the reference value, we observe that the inflection point moves towards the anterior

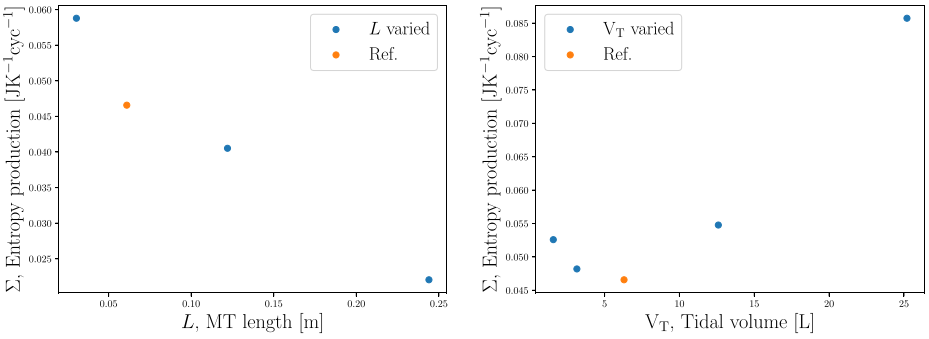

(a) L varied. (b) V_T varied.

Fig. 5. Total entropy production per ventilatory cycle, given T_{amb}= −30 °C when (a) L is varied and (b) V_T is varied. The orange markers represent the reference case.

part of the MT, when measured vs the dimensionless value of $z^* = z/L$. For the chosen values of L, we obtained inflection point positions for inhalation $z^* = 0.36, 0.27, 0.19, 0.07$ from Fig. 4A. A curve with an inflection point around $z^* = 0.27$ will emerge with a plateau at the core body temperature. This happens for the reference case at $z^* > 0.7$. The variations in the reference case, the black lines in Fig. 3A and Fig. 4A, suggest that the normal length of the MT is able to keep the nose sufficiently warm.

The total entropy production is a quantitative measure of the efficiency of the MT as an adsorption/desorption system. The total entropy production per cycle (in JK^{-1}cyc^{-1}) was computed as a function of L and is shown in Fig. 5 as a function of the physiological variables. The variation with tidal volume, V_T, is also shown. The reference case is represented by an orange circle in these figures. Results are also listed in the overview, Table 2.

The profile that illustrates the effects of changes in L in Fig. 5A is a monotonic function. The entropy production, or energy dissipation, shrinks as the MT length increases. Such a dependence on size is well-known; the energy dissipation becomes lower, when there are larger areas available for transfer (Kjelstrup et al., 2017). An MT system that is too long would have implications for skull morphology, which might in turn impact swimming drag or bite mechanics. Also, it would increase resistance to breathing. Such issues are not captured by our model.

Fig. 5B is interesting from an evolutionary perspective. The Σ in this figure is not a monotonic function of V_T. A minimum appears in Σ approximately when V_T is in the vicinity of the assumed reference value of Eb, 6.3 dm^3 in Table 1. A V_T-optimal volume may differ between species, depending on their particular nasal morphology, but V_T is primarily dictated by the need to exchange carbon dioxide for oxygen. In other words, the MT length and structure may have evolved in a direction that involves the least entropy production for heat and water exchange. The flow rate (or V_T) and geometrical characteristics like length L, porosity, or perimeter, γ_a, may interact and together foster a direction for evolution along these lines.

4.8. The breathing frequency

Results from a variation in breathing frequency (at fixed tidal volume) are reported in Fig. 6. We first note that there is no impact of the frequency choice on the temperature profile at maximum flow velocities in Figs. 6B and D. The variation in frequency has an impact on the start (snapshot time $t^* = 0.041$) or on the turning time (snapshot time $t^* = 0.5$) of the cycle. These variations leads to a variation in Σ of more than a factor of three, see Fig. 6E.

The decrease in entropy production which follows from an increasing frequency may be beneficial to the animal under certain circumstances. It may save energy to take frequent, smaller breaths, rather than infrequent deep breaths for inhalation/exhalation. Such a type of process is known to reduce the entropy production in general (Kjelstrup et al., 2017). As seals are maturing, their resting breathing frequency and heart rate typically decrease (Lapierre et al., 2004). The breathing frequency and depth of breathing may decline to half the original value when the weaned pup of gray seals grow into a juvenile stage (Reed et al., 1994). Here we see that smaller breaths can be associated with savings in MT entropy production. However, if increasing the breathing frequency is associated with a reduction in V_T this will result in over-ventilation of anatomical dead-space, which would reduce the efficiency of gas exchange.

We have seen above that a considerable variation takes place in the total entropy production in the MT of *Erignathus barbatus* related to changes in morphology and the manner of breathing. On one hand there could be long-term, growth-dependent changes, like in MT porosity and length. On the other hand, there may be a need for flexibility, to accommodate transient changes in tidal volume, which can occur from one breath to the next. Within the range of values computed in Fig. 6E, there seems to be capacity for both types of changes.

5. Conclusion

We have seen that the maxilloturbinate (MT) structure of the bearded seal can be associated with a high and rather constant retention of water and heat during breathing. The heat retention is systematically smaller, and also more costly to maintain as measured by the entropy production. The analysis was done for the bearded seal in the resting state living under cold ambient (−10 °C) and humid (RH = 0.90) conditions (Case 0). The effect of changes in RH and ambient temperature as well as physiological parameters were studied. Dissipated energy is on the average 5 times higher under cold (−30 °C) than under warm (10 °C) ambient conditions, in a model which does not account for thermo regulation.

Not surprising, we find that actual physiological properties, like the MT length, L the tidal volume, V_T and the breathing frequency, f_a have values that normally ensure efficient function. By efficient function we mean that the MT is long enough to avoid cooling and dehydration of the lungs. A minimum is observed in the entropy production vs V_T when V_T is near its base case value. The minimum suggests that the breathing under these conditions is cost-effective in terms of heat and water retention.

We speculate that a reduction in MT porosity in Eb will improve conditions for heat (and maybe also water) exchange further. We have seen before (Cheon et al., 2023) that the entropy production in the MT of Eb is lower than in monk seals when both are placed under Arctic conditions. We related this finding to the presence of a larger perimeter of the cross sectional area for air flow in Eb, associated with a smaller MT porosity. The variations in entropy production align with the losses in heat and water, and support the idea that the MT provides a heat and water exchange system which is tailored for the purpose.

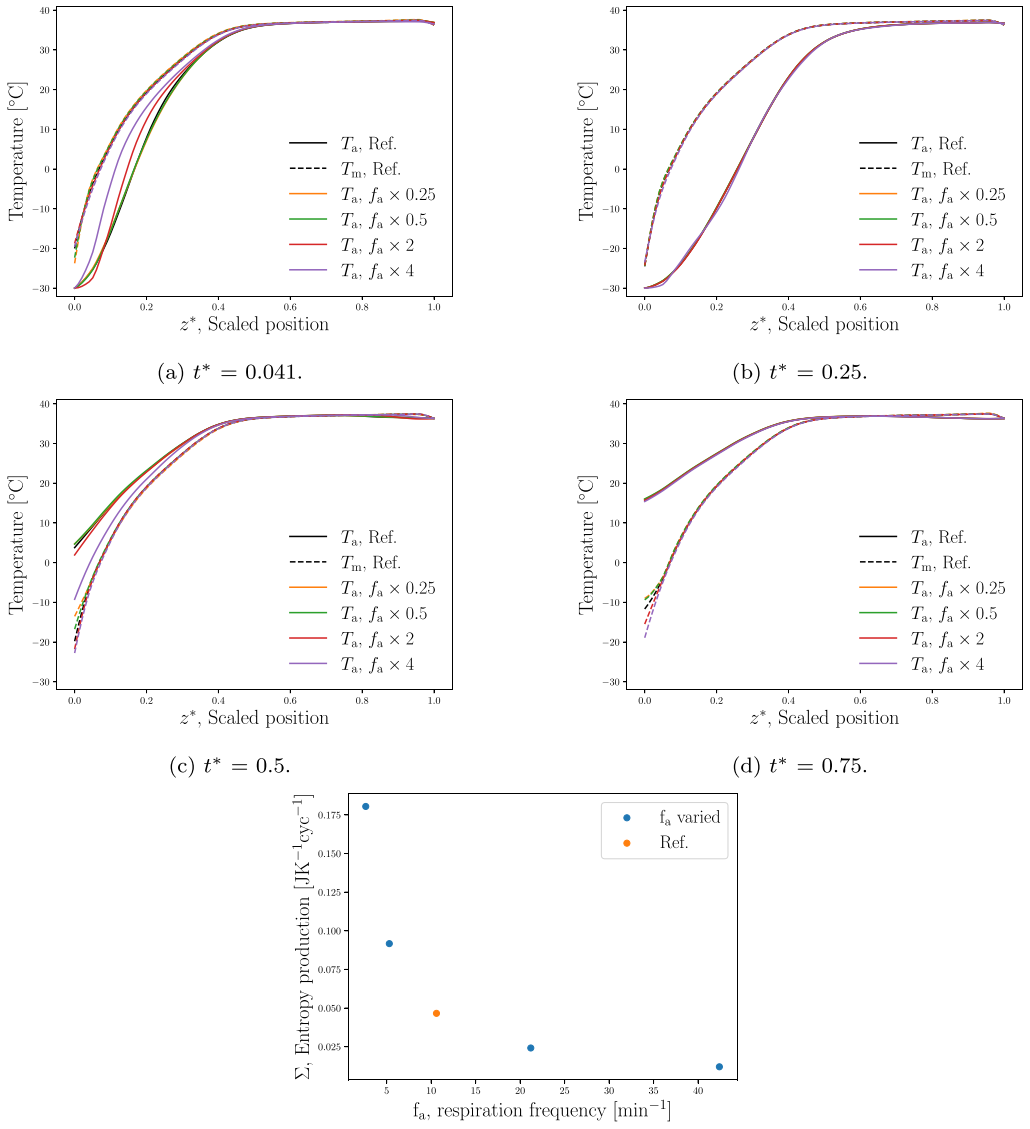

Fig. 6. Temperature profiles of air (solid line) and mucus (dashed line) subsystems regarding f_a variation when (a) $t^* = 0.042$, (b) $t^* = 0.25$, (c) $t^* = 0.5$ and (d) $t^* = 0.75$. (e) Total entropy production per ventilatory cycle, given $T_{amb} = -30$ °C when f_a varied. The orange markers represent the reference case.

CRediT authorship contribution statement

Hyejeong Lee Cheon: Writing – original draft, Visualization, Validation, Investigation, Formal analysis, Conceptualization. **Nataliya Kizilova:** Writing – review & editing, Supervision, Formal analysis, Conceptualization. **Eirik G. Flekkøy:** Writing – review & editing, Funding acquisition. **Matthew J. Mason:** Writing – review & editing, Formal analysis. **Lars P. Folkow:** Writing – review & editing, Formal analysis. **Signe Kjelstrup:** Writing – review & editing, Writing – original draft, Validation, Supervision, Project administration, Investigation, Funding acquisition, Formal analysis, Conceptualization.

Declaration of competing interest

The authors declare that the research was conducted in the absence of any commercial or financial relationships that could be constructed as a potential conflict of interest.

Data availability

Codes that are used this work are available at https://github.com/hyejeonc/nose-calculations.

Acknowledgments

HLC is grateful to the Faculty of Science, Norwegian University of Science and Technology. SK and HLC are grateful to the Research Council of Norway, Center of Excellence Funding Scheme, project no 262644 PoreLab. HLC is grateful for supervision from Kathrine Røe Redalen.

Appendix. Hydrodynamic variables

Two dimensionless hydrodynamic numbers, the Reynolds and Womersley numbers, Re and Wo, are central for the fluid dynamic performance of the nasal turbinate. The numbers determine the solution of the Navier–Stokes equation. Reynolds number is a measure of the ratio of inertia to viscous forces, and indicates the likelihood for *turbulence*.

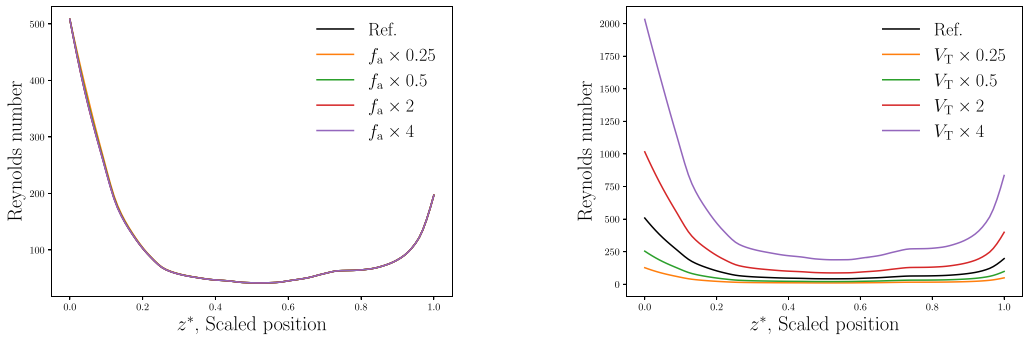

(a) Re by varied f_a when $t^* = 0.25$. (b) Re by varied V_T when $t^* = 0.25$.

Fig. 7. Re as a function of scaled position when (a) f_a is varied and (b) V_T is varied.

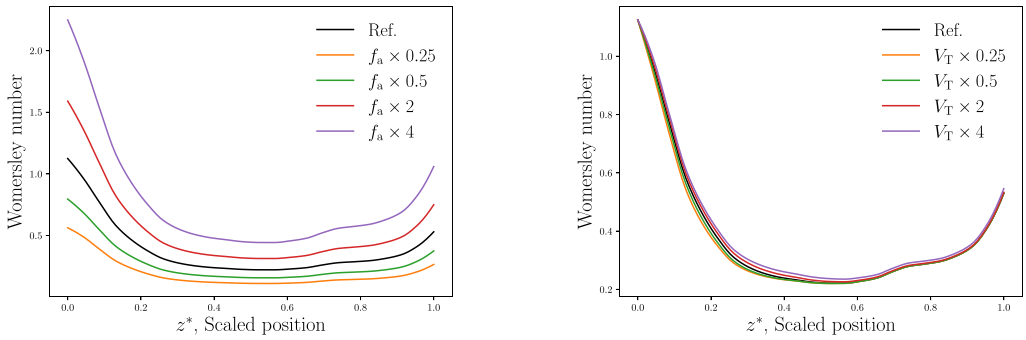

(a) Wo for various f_a, $t^* = 0.25$. (b) Wo for various V_T, $t^* = 0.25$.

Fig. 8. Wo as a function of scaled position when (a) f_a is varied and (b) V_T is varied.

A flow with Re > 4000 is considered to be in the turbulence regime. When Re < 2300, the flow is considered to be in the laminar regime. The Womersley number refers to the *unsteadiness* of the flow in response to an unsteady pressure gradient. When Wo < 1, a flow is considered to be quasi-steady. The flow becomes transient flow when Wo grows from 1 (Loudon and Tordesillas, 1998). When the Reynolds number exceeds a critical value 2100–4000 depending on the fluid (Wang, 2005), a turbulent flow could be developed. It is known from estimations on different animals, that laminar or transitional laminar-to-turbulent flow can be observed in nasal ducts cf. Craven et al. (2007), Magnanelli et al. (2017), Solberg et al. (2020).

The Reynolds number (Re) and the Womersley number (Wo) are defined as,

$$\mathrm{Re} = \frac{v_a D_h}{\nu}, \tag{15}$$

$$\mathrm{Wo} = \frac{D_h}{2}\sqrt{\frac{2\pi f_a}{\nu}}, \tag{16}$$

Here v_a is the velocity of air flow, ν is the kinematic viscosity and f_a is the air respiration frequency in Hz. The hydraulic diameter, D_h, is the characteristic airway diameter (width) which enter the expressions for both Re and Wo. It is given by,

$$D_h = \frac{4A_a}{\gamma_a}, \tag{17}$$

where A_a is the cross-sectional area and γ_a is the perimeter of the air pathway.

Fig. 7A show snapshots of Re vs. f_a when $t^* = 0.25$, and the velocity of airflow has its maximum. Fig. 7B shows Re varies with V_T. There is a plateau at $0.2 < z^* < 0.7$. Re is below 2000 for all z^* range in Fig. 7A and B which indicates all airflow is probably laminar rather than turbulent.

The change in Wo with f_a is shown in Fig. 8A. The Wo is greatest when f_a is ×4. A variation in V_T has no impact, see Fig. 8B. The largest numbers are obtained at the end of a nose, for example, $z^* \approx 0,1$. We conclude that the flow is stable in the oscillating pressure field.

References

Blix, A.S., 2016. Adaptations to polar life in mammals and birds. J. Exp. Biol. 219 (8), 1093–1105.

Blix, A.S., Johnsen, H.K., 1983. Aspects of nasal heat exchange in resting reindeer. J. Physiol. 340 (1), 445–454.

Bush, M.L., Frederick, C.B., Kimbell, J.S., Ultman, J.S., 1998. A CFD-PBPK hybrid model for simulating gas and vapor uptake in the rat nose. Toxicol. Appl. Pharmacol. 150 (1), 133–145.

Cameron, M.F., Frost, K.J., Ver Hoef, J.M., Breed, G.A., Whiting, A.V., Goodwin, J., Boveng, P.L., 2018. Habitat selection and seasonal movements of young bearded seals (Erignathus barbatus) in the Bering Sea. PLoS One 13 (2), e0192743.

Castellini, M.A., Milsom, W.K., Berger, R.J., Costa, D.P., Jones, D.R., Castellini, J.M., Rea, L.D., Bharma, S., Harris, M., 1994. Patterns of respiration and heart rate during wakefulness and sleep in elephant seal pups. Am. J. Physiol.-Regul., Integrat. Comparat. Physiol. 266 (3), R863–R869.

Cheon, H.L., Kjelstrup, S., Kizilova, N., Flekkøy, E.G., Mason, M.J., Folkow, L.P., 2023. Structure-function relationships in the nasal cavity of Arctic and subtropical seals. Biophys. J. 122 (24), 4686–4698.

Craven, B.A., Neuberger, T., Paterson, E.G., Webb, A.G., Josephson, E.M., Morrison, E.E., Settles, G.S., 2007. Reconstruction and morphometric analysis of the nasal airway of the dog (Canis familiaris) and implications regarding olfactory airflow. Anat. Rec.: Adv. Integr. Anat. Evol. Biol.: Adv. Integr. Anat. Evol. Biol. 290 (11), 1325–1340.

Craven, B.A., Paterson, E.G., Settles, G.S., 2010. The fluid dynamics of canine olfaction: unique nasal airflow patterns as an explanation of macrosmia. J. R. Soc. Interface 7 (47), 933–943.

Elad, D., Wolf, M., Keck, T., 2008. Air-conditioning in the human nasal cavity. Respir. Physiol. Neurobiol. 163 (1–3), 121–127.

Escobar-Amado, C.D., Badiey, M., Pecknold, S., 2022. Automatic detection and classification of bearded seal vocalizations in the northeastern Chukchi Sea using convolutional neural networks. J. Acoust. Soc. Am. 151 (1), 299–309.

Flekkøy, E.G., Folkow, L.P., Kjelstrup, S., Mason, M.J., Wilhelmsen, Ø., 2023. Thermal modeling of the respiratory turbinates in arctic and subtropical seals. J. Therm. Biol. 112, 103402.
Folkow, L.P., Blix, A.S., 1987. Nasal heat and water exchange in gray seals. Am. J. Physiol.-Regul., Integr. Compar. Physiol. 253 (6), R883–R889.
Folkow, L., Blix, A., Eide, T., 1988. Anatomical and functional aspects of the nasal mucosal and ophthalmic retia of phocid seals. J. Zool. 216 (3), 417–436.
Foster, G., Nymo, I.H., Kovacs, K.M., Beckmen, K.B., Brownlow, A.C., Baily, J.L., Dagleish, M.P., Muchowski, J., Perrett, L.L., Tryland, M., et al., 2018. First isolation of Brucella pinnipedialis and detection of Brucella antibodies from bearded seals Erignathus barbatus. Dis. Aquat. Org. 128 (1), 13–20.
Garcia, G.J., Bailie, N., Martins, D.A., Kimbell, J.S., 2007. Atrophic rhinitis: a CFD study of air conditioning in the nasal cavity. J. Appl. Physiol. 103 (3), 1082–1092.
Hanna, L., Scherer, P., 1986. Regional control of local airway heat and water vapor losses. J. Appl. Physiol. 61 (2), 624–632.
Hillenius, W.J., 1992. The evolution of nasal turbinates and mammalian endothermy. Paleobiology 18 (1), 17–29.
Huntley, A.C., Costa, D.P., Rubin, R.D., 1984. The contribution of nasal countercurrent heat exchange to water balance in the northern elephant seal, Mirounga angustirostris. J. Exp. Biol. 113 (1), 447–454.
Ito, K., Mitsumune, K., Kuga, K., Phuong, N.L., Tani, K., Inthavong, K., 2017. Prediction of convective heat transfer coefficients for the upper respiratory tracts of rat, dog, monkey, and humans. Indoor Built Environ. 26 (6), 828–840.
Jackson, D., Scmidt-Nielsen, K., 1964. Countercurrent heat exchange in the respiratory passages. Proc. Natl. Acad. Sci. USA 1192–1197.
Johannessen, E., Kjelstrup, S., 2004. Minimum entropy production rate in plug flow reactors: An optimal control problem solved for SO2 oxidation. Energy 29 (12–15), 2403–2423.
Johansen, K., Bech, C., 1983. Heat conservation during cold exposure in birds (vasomotor and respiratory implications). Polar Res. 1 (3), 259–268.
Kaulbach, H.C., White, M.V., Igarashi, Y., Hahn, B.K., Kaliner, M.A., 1993. Estimation of nasal epithelial lining fluid using urea as a marker. J. Allergy Clin. Immunol. 92 (3), 457–465.
Kim, D.-W., Chung, S.-K., Na, Y., 2017. Numerical study on the air conditioning characteristics of the human nasal cavity. Comput. Biol. Med. 86, 18–30.
Kings, J.E., Folkow, L.P., Hammer, O., Kjelstrup, S., Mason, M.J., Xiong, F., Flekkoy, E.G., 2023. A model for maxilloturbinate morphogenesis in seals. bioRxiv 2023-12.
Kjelstrup, S., Bedeaux, D., Johannessen, E., Gross, J., 2017. Non-Equilibrium Thermodynamics for Engineers. World scientific.
Kjelstrup, S., de Koeijer, G.M., 2003. Transport equations for distillation of ethanol and water from the entropy production rate. Chem. Eng. Sci. 58 (7), 1147–1161.
Langman, V., 1985. Nasal heat exchange in a northern ungulate, the reindeer (Rangifer tarandus). Respir. Physiol. 59 (3), 279–287.
Lapierre, J.L., Schreer, J.F., Burns, J.M., Hammill, M.O., 2004. Developmental changes in cardiorespiratory patterns associated with terrestrial apnoeas in harbour seal pups. J. Exp. Biol. 207 (22), 3891–3898.
Llobet, S.M., Ahonen, H., Lydersen, C., Berge, J., Ims, R., Kovacs, K.M., 2021. Bearded seal (Erignathus barbatus) vocalizations across seasons and habitat types in Svalbard, Norway. Polar Biol. 44 (7), 1273–1287.
Loudon, C., Tordesillas, A., 1998. The use of the dimensionless womersley number to characterize the unsteady nature of internal flow. J. Theoret. Biol. 191 (1), 63–78.
Lydersen, C., Kovacs, K., Hammill, M., Gjertz, I., 1996. Energy intake and utilisation by nursing bearded seal (Erignathus barbatus) pups from Svalbard, Norway. J. Compar. Physiol. B 166, 405–411.
MacIntyre, K.Q., Stafford, K.M., Berchok, C.L., Boveng, P.L., 2013. Year-round acoustic detection of bearded seals (Erignathus barbatus) in the Beaufort Sea relative to changing environmental conditions, 2008–2010. Polar Biol. 36, 1161–1173.
Magnanelli, E., Wilhelmsen, Ø., Acquarone, M., Folkow, L.P., Kjelstrup, S., 2017. The nasal geometry of the reindeer gives energy-efficient respiration. J. Non-Equilib. Thermodyn. 42 (1), 59–78.
Marks, T.N., Maddux, S.D., Butaric, L.N., Franciscus, R.G., 2019. Climatic adaptation in human inferior nasal turbinate morphology: Evidence from Arctic and equatorial populations. Am. J. Phys. Anthropol. 169 (3), 498–512.
Marshall, C.D., Amin, H., Kovacs, K.M., Lydersen, C., 2006. Microstructure and innervation of the mystacial vibrissal follicle-sinus complex in bearded seals, Erignathus barbatus (Pinnipedia: Phocidae). Anat. Rec. A: Discov. Mol. Cell. Evol. Biol.: Off. Publ. Am. Assoc. Anat. 288 (1), 13–25.
Mason, M.J., Wenger, L.M., Hammer, Ø., Blix, A.S., 2020. Structure and function of respiratory turbinates in phocid seals. Polar Biol. 43 (2), 157–173.
Moore, C.L., 1981. An olfactory basis for maternal discrimination of sex of offspring in rats (Rattus norvegicus). Animal Behav. 29 (2), 383–386.
Naftali, S., Rosenfeld, M., Wolf, M., Elad, D., 2005. The air-conditioning capacity of the human nose. Ann. Biomed. Eng. 33, 545–553.
Negus, V., 1958. Ace Hold the Comparative Anatomy and Physiology of the Nose and Paranasal Sinuses. E. & S. Livingstone.
Olnes, J., Crawford, J., Citta, J., Druckenmiller, M., Von Duyke, A., Quakenbush, L., 2020. Movement, diving, and haul-out behaviors of juvenile bearded seals in the Bering, Chukchi and Beaufort seas, 2014–2018. Polar Biol. 43, 1307–1320.
Rauter, M.T., Schnell, S.K., Hafskjold, B., Kjelstrup, S., 2021a. Thermo-osmotic pressure and resistance to mass transport in a vapor-gap membrane. Phys. Chem. Chem. Phys. 23 (23), 12988–13000.
Rauter, M.T., Schnell, S.K., Kjelstrup, S., 2021b. Cassie–baxter and wenzel states and the effect of interfaces on transport properties across membranes. J. Phys. Chem. B 125 (46), 12730–12740.
Reed, J., Chambers, C., Fedak, M., Butler, P., 1994. Gas exchange of captive freely diving grey seals (Halichoerus grypus). The J. Exp. Biol. 191 (1), 1–18.
Reynolds, H., Seaman, G., 1976. The natural history and ecology of the bearded seal (Erignathus barbatus) and the ringed seal (Phoca (Pusa) hispida). Annual Report Contract 03-5-022-53, Fairbanks, Alaska, p. 31.
Solberg, S.B.B., Kjelstrup, S., Magnanelli, E., Kizilova, N., Barroso, I.L.C., Acquarone, M., Folkow, L.P., 2020. Energy efficiency of respiration in mature and newborn reindeer. J. Compar. Physiol. B 190, 509–520.
Thometz, N.M., Hermann-Sorensen, H., Russell, B., Rosen, D.A., Reichmuth, C., 2021. Molting strategies of Arctic seals drive annual patterns in metabolism. Conserv. Physiol. 9 (1), coaa112.
Wang, C., 2005. Chapter 3 airflow in the respiratory system. In: Interface Science and Technology; Inhaled Particles. 5, Elsevier, Amsterdam, the Netherlands, pp. 31–54.
Westvik, M.A., 2022. The structure of nasal conchae in Svalbard rock ptarmigan (Lagopus muta hyperborea) with comparisons to three other Galliform birds. (Master's thesis). UiT Norges arktiske universitet.
Wilhelmsen, Ø., Trinh, T.T., Lervik, A., Badam, V.K., Kjelstrup, S., Bedeaux, D., 2016. Coherent description of transport across the water interface: From nanodroplets to climate models. Phys. Rev. E 93 (3), 032801.